RSC Advances

PAPER

View Article Online
View Journal | View Issue

Check for updates

Cite this: *RSC Adv.*, 2017, **7**, 41779

Endocytosis mechanism of a novel proteoglycan, extracted from *Ganoderma lucidum*, in HepG2 cells

Zhou Yang,[a] Fan Wu,[a] Hongjie Yang[b] and Ping Zhou *[a]

Received 8th July 2017
Accepted 11th August 2017

DOI: 10.1039/c7ra07520k

rsc.li/rsc-advances

A novel protein tyrosine phosphatase 1B (PTP1B) inhibitor, *FYGL*, extracted from *Ganoderma lucidum*, was first reported to have an efficient hypoglycemic effect and high safety *in vivo* in our previous study. However, the underlying mechanism of the anti-diabetes activity was still unclear. The dominant effective component of *FYGL* was demonstrated to be a neutral hyperbranched proteoglycan macromolecule. Therefore, it is necessary to first elucidate how the biomacromolecule works at the cellular level, in order to understand its possible functional mechanism *in vivo*. Herein, we focused on demonstrating the cell internalization and endocytosis mechanism of *FYGL* in HepG2 cells. A series of cellular uptake pathways was explored, including clathrin-mediated endocytosis, caveolae/lipid-mediated endocytosis, and macropinocytosis. Confocal laser scanning microscopy and flow cytometry were used to demonstrate the absorption of *FYGL* by HepG2 cells. Furthermore, pharmacologically selective inhibitors and Western blot methods were used to demonstrate that macropinocytosis mediated by c-Src/PI3K cascades was the preferred route for the uptake of *FYGL* in cells. Our study provided the basis of uptake of *FYGL* for an efficient hypoglycemic effect. The functional mechanism of the signaling pathway *in vivo* will be reported in the future.

Open Access Article. Published on 29 August 2017. Downloaded on 2/15/2026 8:58:24 PM.
This article is licensed under a Creative Commons Attribution-NonCommercial 3.0 Unported Licence.

1. Introduction

The protein tyrosine phosphatase 1B (PTP1B), a member of the protein tyrosine phosphatase (PTPs) family, is overexpressed in insulin-sensitive peripheral tissues, such as liver and muscle tissues, in type 2 diabetes mellitus (T2DM) patients; it negatively regulates the insulin signaling pathway by dephosphorylating insulin receptor substrate (IRS) on tyrosine residues.[1,2] Inhibiting PTP1B activity is considered an efficient strategy for the management of T2DM. Therefore, identifying PTP1B inhibitors is a topic of current interest; however, no ideal inhibitor has been found for clinical use thus far, because of either poor bioavailability or low safety.[3,4] Interestingly, our previous study found a novel PTP1B inhibitor, *FYGL*, which was extracted from *Ganderma lucidum*, a well-known Chinese medicinal fungus that has long been used as a traditional Chinese medicine.[5,6] The molecular weight of *FYGL* is 2.6×10^5, and the structure of the dominant component is shown in Fig. 1. *FYGL* is an amphiphilic hyperbranched proteoglycan consisting of hydrophilic polysaccharides (4 saccharide units) and lipophilic protein moieties (17 amino acids) with a ratio of 77 : 17 for saccharide : protein.[7] We first demonstrated that *FYGL* has an efficient hypoglycemic effect and high safety *in vivo*,[5] but mechanism was still unclear. In order to understand the possible functional mechanism of *FYGL*, it is necessary to first reveal how the biomacromolecule works at the cellular level. Therefore, herein, we focused on demonstrating the cell internalization and endocytosis mechanism of *FYGL* in HepG2 cells, which are engaged in glycogen synthesis.

Cell internalization of a macromolecular drug involves specific or multiple endocytosis processes.[8] Endocytosis is a process involving the uptake of particles, fluids and macromolecules from the outside to the inside of a cell.[9] The endocytosis mechanisms mainly include clathrin-mediated endocytosis (CME) and clathrin-independent endocytosis (CIE); the latter involves caveolae/lipid-mediated endocytosis and macropinocytosis.[9] Endocytic pathways are key to current drug delivery strategies and functional materials used in the field of biomedicine.[10] Macropinocytosis was first observed in 1931, representing a distinct endocytic pathway in mammalian cell lines,[11,12] and can contribute to the efficiency by which numerous cell-penetrating peptides translocate to the cytoplasm.[13] This process is an actin-dependent endocytic pathway and occurs through large vesicles of variable sizes (diameter 0.2–5 μm) called macropinosomes.[14] As a typical macropinocytosis tracer, dextran is often used to co-localize with the studied drug in cells for proving the macropinocytosis mechanism.[15] A protein tyrosine kinase implicated in cancer and some intracellular signaling cascades,[16] c-sarcomagene (c-Src), can promote cell proliferation and inhibit cell apoptosis *via* PI3K/Akt cascades.[17] In the initial stage of macropinocytosis, c-Src

[a]*State Key Laboratory of Molecular Engineering of Polymers, Department of Macromolecular Science, Fudan University, Shanghai 200433, P. R. China. E-mail: pingzhou@fudan.edu.cn; Fax: +86-21-55664038; Tel: +86-21-55664038*

[b]*Yueyang Hospital of Integrated Traditional Chinese and Western Medicine, Shanghai University of Traditional Chinese Medicine, Shanghai 200437, P. R. China*

Open Access Article. Published on 29 August 2017. Downloaded on 2/15/2026 8:58:24 PM.
This article is licensed under a Creative Commons Attribution-NonCommercial 3.0 Unported Licence.

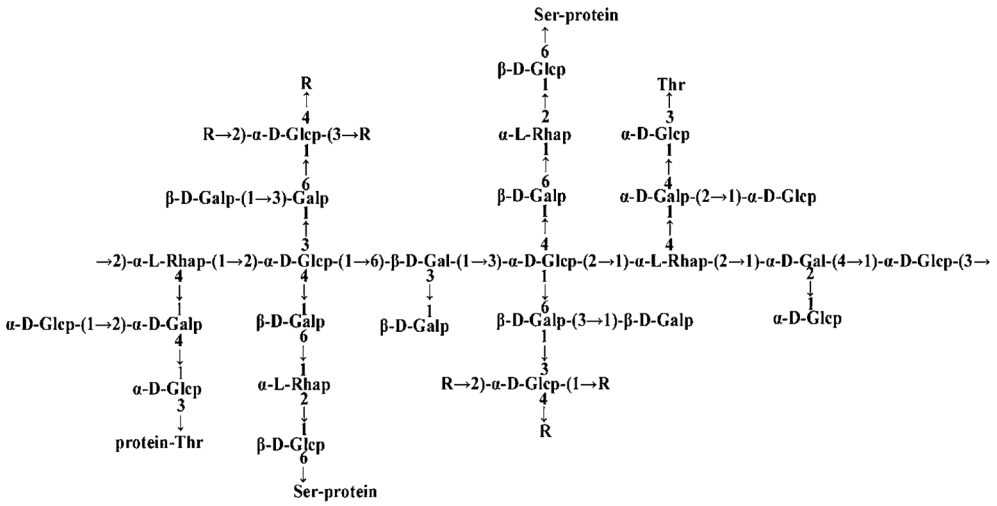

Fig. 1 The structure of *FYGL* (Ara: arabinose, Gal: galactose, Glc: glucose, Rha: rhamnose, Thr: threonine, Ser: serine). The suffixes p and f represent pyranose and furanose, respectively.

induces cell ruffling and influences the cell shape, following which it closes the outermost margin to form a vesicle.[18]

Pharmacologically selective inhibitors are generally used to study the mechanism of endocytosis.[9] Among the inhibitors, chlorpromazine can inhibit clathrin-mediated endocytosis but not specifically during the process.[19] Nystatin can decompose cholesterol, and thus inhibit caveolae/lipid-mediated endocytosis.[20] Amiloride negatively influences macropinocytosis.[21] Genistein mediates some kinases involved in endocytosis,[22] and LY294002 is a common inhibitor of phosphatidylinositol-3 kinase (PI3K), which regulates macropinocytosis and RhoA-mediated endocytosis, a member of the Ras homolog gene family.[23]

In the present study, we attempt to reveal the specific endocytosis process through which *FYGL* enters the HepG2 cells, for drug uptake. A clear understanding of the endocytosis mechanism of *FYGL* at the cellular level will shed light on the roles of traditional natural macromolecular products in medicine.

2. Materials and methods

2.1 Materials

FYGL was extracted from *Ganderma lucidum* in our laboratory.[5] Dulbecco's modified Eagle's medium (DMEM), opti-minimal essential medium (opti-MEM) and fetal bovine serum (FBS) were purchased from Gibco Co. Ltd. (USA). Paraformaldehyde (4%), penicillin and streptomycin were purchased from Sangon Co. Ltd. (Shanghai, China). Cell counting kit-8 (CCK-8) was acquired from Dojindo Co. Ltd. (Shanghai, China). Fluorescein isothiocyanate (FITC), 4′,6-diamidino-2-phenylindole (DAPI), chlorpromazine, nystatin, genistein and amiloride were obtained from Aladdin Co. Ltd. (Shanghai, China). Rhodamine-phalloidin, a protein marker of FBS and polylysine were sourced from Yeasen Co. Ltd. (Shanghai, China). RIPA lysis buffer, lipofectamine 6000 and LY294002 were purchased from Beyotime Co. Ltd. (Shanghai, China). Tetramethylrhodamine isothiocyanate (TRITC) labeled-dextran was purchased from Xibao Co. Ltd. (Shanghai, China). HepG2 cell lines were provided by Fuxiang Co. Ltd. (Shanghai, China).

2.2 Oil/water (O/W) partition coefficient determination

Octanol and water were mixed and shaken vigorously to form two phases of water-saturated octanol (oil phase, phase-O) and octanol-saturated water (water phase, phase-W). The concentration of *FYGL* in phase-W was measured by the bicinchoninic acid (BCA) assay for protein analysis. *FYGL* was dissolved in phase-O to form 250 μg mL^{-1} solution. A given volume of phase-O was mixed with phase-W, and the mixture was shaken at 30 °C until the distribution of *FYGL* attained equilibrium in the two phases. Finally, the O/W partition coefficient (K_{OW}) was calculated based on eqn (1):[24]

$$K_{OW} = \frac{C_O V_O - C_W V_W}{C_W V_O} \quad (1)$$

where C_O is the original concentration of *FYGL* in phase-O, V_O is the volume of phase-O, C_W is the equilibrium concentration of *FYGL* in phase-W, and V_W is the volume of phase-W.

2.3 Measurement of *FYGL* particle size

A solution of *FYGL* (2 mg mL^{-1}) was prepared in phosphate buffered solution (PBS), and the particle size measured by Zetasizer Nano (Malvern, UK).

2.4 Cell culture

HepG2 cells were cultured in DMEM supplement with 10% FBS and 1% penicillin–streptomycin at 37 °C, in 5% CO_2 atmosphere.

 This journal is © The Royal Society of Chemistry 2017

Open Access Article. Published on 29 August 2017. Downloaded on 2/15/2026 8:58:24 PM.
This article is licensed under a Creative Commons Attribution-NonCommercial 3.0 Unported Licence.

2.5 CCK-8 test

HepG2 cells were seeded into 96-well plates, and then endocytic selective inhibitors (with different concentrations in DMEM with 2% FBS) were added into the wells and incubated for 4.5 h at 37 °C. CCK-8 was added and cultured for another 0.5–2 h. Each sample was replicated in three wells. Finally the optical density (OD) was measured at 450 nm by a microplate reader (Bio-Tek, USA) and the cell viability was calculated.

2.6 Intracellular uptake of *FYGL*

FYGL was labeled by a green fluorescence marker, FITC, to form *FITC-FYGL* by the following procedure. FITC (1 mg) was dissolved in 1 mL DMSO, and the solution was added into sodium buffer containing 1 mg mL^{-1} *FYGL* at a volume ratio of 1 to 10. This mixture was stirred for 24 h at 4 °C, away from light, to form the *FITC-FYGL* solution. HepG2 cells were transferred into 12-well plates and incubated with the *FITC-FYGL* solution for 6 h, then washed with PBS, fixed with 4% paraformaldehyde, permeated with 0.2% Triton X-100/PBS, and stained with DAPI for the cellular nucleus and rhodamine-phalloidin for the cytoskeleton. The HepG2 cells were finally mounted on the glass slide for observation of the uptake of *FYGL* in by a confocal laser scanning microscope (C2+, Nikon, Japan). In addition, the HepG2 cells were also transferred into 6-well plates at a density of 5×10^5 to 1×10^6 cells per well and incubated with *FITC-FYGL* at different concentrations for 6 h; the cell suspensions were then analyzed by flow cytometry (Gallios, Beckman coulter, USA) at channel FL1 (excitation wavelength at 488 nm and emission wavelength at 525 nm) to demonstrate the absorption of *FYGL* by the HepG2 cells.

2.7 Endocytic inhibition of *FYGL* in HepG2 cells

HepG2 cells were transferred into 6-well plates with a density of 5×10^5 to 1×10^6 cells per well, pre-incubated with endocytic selective inhibitors at safe concentrations for 0.5 h, and then incubated with *FITC-FYGL* at the indicated concentration for 4 h. Finally, the cell suspensions were analyzed by flow cytometry at channel FL1 and observed by confocal laser scanning microscope with the same protocol as described in part 2.6.

2.8 *FYGL* in HepG2 cells transfected by c-Src siRNA

HepG2 cells were seeded into 6-well plates. A mixture solution of 20 μM c-Src siRNA (synthesized by Sangon Bio. Co, sequence shown in Table 1) and 5 μL lipofectamine 6000 were premixed in opti-MEM and added into the wells. The solution was removed 6 h later and the cells were washed thrice with PBS. A solution of *FITC-FYGL* at the indicated concentration in DMEM with 2% FBS was added into the wells and incubated for 4 h at 37 °C, followed by analysis of FCM and confocal laser scanning microscopy.

Table 1 The c-Src siRNA sequence

Sense (5′ to 3′)	CAAGAGCAAGCCCAAGGAU
Anti-sense (5′ to 3′)	AUCCUUGGGCUUGCUCUUG

2.9 c-Src protein extraction and Western blot

HepG2 cells were lysed in RIPA lysis buffer (Beyotime Co. Ltd) and clarified by centrifugation (12 000 × *g*, 10 min, 4 °C). The cell lysates were separated by 8% SDS-PAGE, transferred to a polyvinylidene fluoride (PVDF) membrane, and then immunoblotted with rabbit polyclonal c-Src antibody (Sangon Co, Shanghai, China) and secondary goat anti-rabbit antibody (Cell Signaling Technology, USA). Bands were visualized with enhanced chemiluminescence solution (ECL, Biotanon) and detected by Image Lab camera (Bio-Rad, Germany); they were then quantified by densitometry scanning by the Image J software.

2.10 Intracellular co-localization of *FYGL* and dextran

HepG2 cells were seeded at a density of 2×10^4 cells per well; to these cells 100 μg mL^{-1} *FITC-FYGL* was added and incubated for 4 h. Following this, the medium was removed, TRITC-dextran was added and incubated for 10 min, and then the cells were fixed with 4% paraformaldehyde and observed by a confocal laser scanning microscope.

2.11 Statistical analysis

All data were presented as mean ± SD. One-way ANOVA test was performed to analyze the statistical significance between the two groups. A difference is considered to be statistically significant when the p value was <0.05.

3. Results and discussion

3.1 Oil/water (O/W) partition coefficient of *FYGL*

A working drug should possess amphiphilic properties in order to be transported in the human body and penetrate into the cell membrane. The oil/water partition coefficient is an important

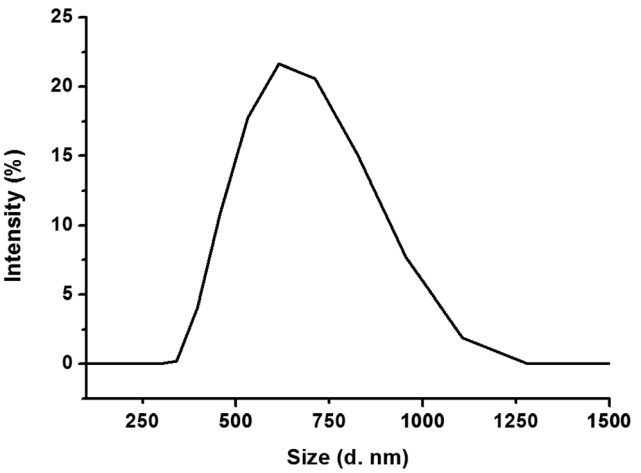

Fig. 2 The particle size distribution of *FYGL* in water at room temperature. Data are presented as mean ± SD ($n = 3$).

Open Access Article. Published on 29 August 2017. Downloaded on 2/15/2026 8:58:24 PM.
This article is licensed under a Creative Commons Attribution-NonCommercial 3.0 Unported Licence.

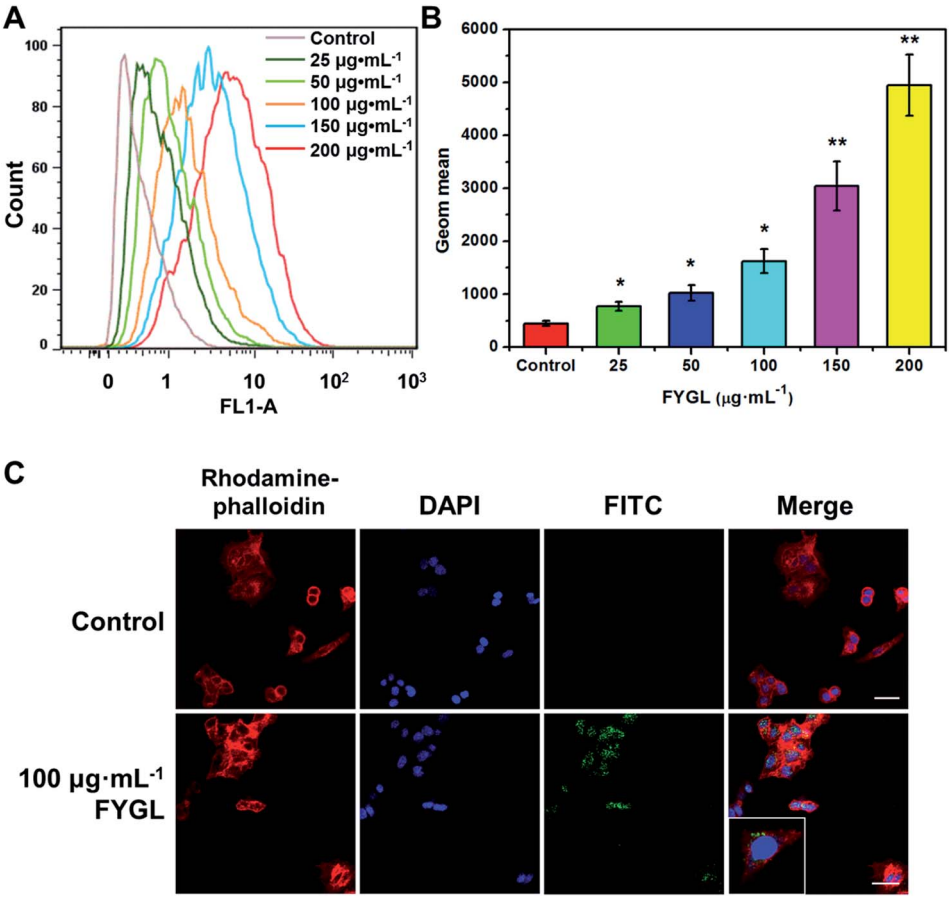

Fig. 3 (A) FCM shows the peak position of *FITC-FYGL* at the designated concentrations (incubation for 6 h at 37 °C) in channel FL1. (B) The Geom. mean reflects the relative fluorescent intensity of *FITC-FYGL* at different concentrations in HepG2 cells. (C) Confocal laser scanning microscopy images of the HepG2 cells after incubation with *FITC-FYGL* for 4 h. The scale bar represents 50 μm. The blue (DAPI labelled), red (rhodamine labelled) and green (FITC labelled) colors represent the cell nucleus, cell cytoskeleton, and *FYGL*, respectively. The inset shows the enlarged cell containing *FYGL* (green). Data are presented as mean ± SD ($n = 3$). *$p < 0.05$, **$p < 0.01$ *versus* the former group.

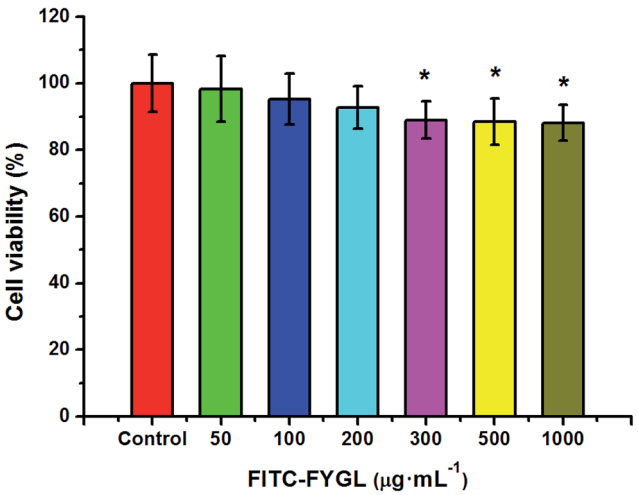

Fig. 4 *In vitro* cell viability of HepG2 cells incubated with different concentrations of *FITC-FYGL* for 24 h at 37 °C. Data are presented as mean ± SD ($n = 6$). *$p < 0.05$ *versus* the control group.

index for the amphiphilic property of a compound. The equilibrium concentration of *FYGL* in phase-W was obtained according to the standard curve plotted by the BCA assay. The partition coefficient K_{ow} of *FYGL*, calculated from eqn (1), was 1.29 ± 0.08, larger than 1.0, suggesting that *FYGL* is soluble in lipids to some extent, in addition to water. It is thus possibly capable of penetrating through cell membranes and entering cells,[25] and the structure of hydrophilic polysaccharide and lipophilic protein moieties including 17 amino acid residuals play an important role in cell penetration, especially the side chain of particular serine/threonine or tyrosine residues which are related to phosphorylation.[26]

Table 2 CCK-8 test of safe concentrations on HepG2 cells

Agent	Safe concentration (μg mL^{-1})
Chlorpromazine	50
Nystatin	50
Amiloride	100
LY294002	10
Genistein	500
FITC-FYGL	200

This journal is © The Royal Society of Chemistry 2017

Open Access Article. Published on 29 August 2017. Downloaded on 2/15/2026 8:58:24 PM.
This article is licensed under a Creative Commons Attribution-NonCommercial 3.0 Unported Licence.

3.2 Particle size of *FYGL*

Fig. 2 shows the particle size distribution of *FYGL* in water at room temperature. The particle size of *FYGL* is mainly distributed in the range 400–1000 nm, and polydispersity index (PDI) is 0.57 ± 0.03, suggesting that *FYGL* exists as aggregated particles in aqueous solution. Thus, the uptake of *FYGL* in cells maybe based on the mechanism of macropinocytosis in which the macropinocytic vesicles can endocytose the particles in the size range 200–5000 nm.

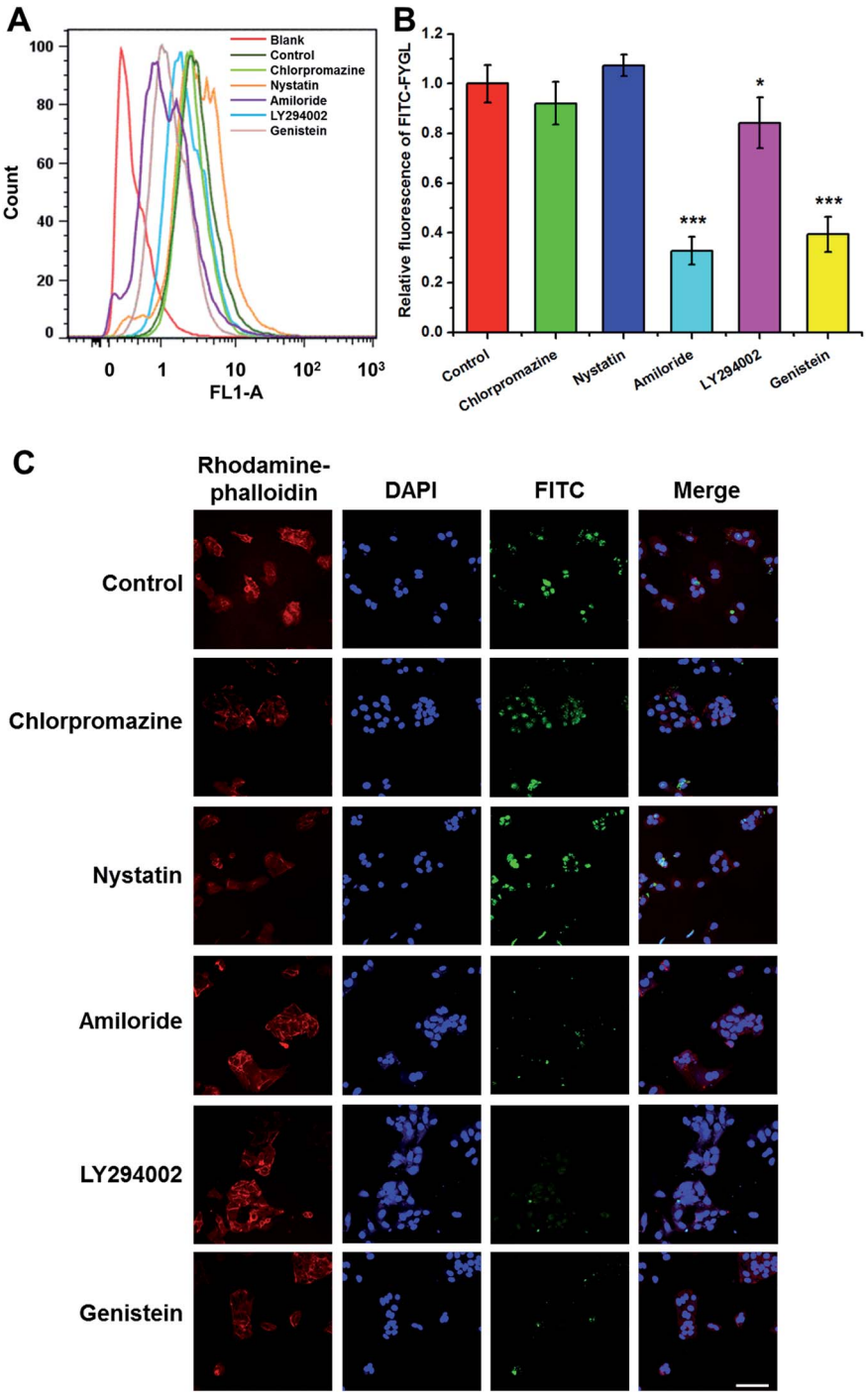

Fig. 5 (A) FCM shows the peak position of 100 μg mL^{-1} *FITC-FYGL* with the selective inhibitor (chlorpromazine, nystatin, amiloride, LY294002, and genistein) in channel FL1. (B) The relative fluorescent intensity of *FITC-FYGL* with the selective inhibitors in HepG2 cells. Data are presented as mean ± SD ($n = 3$). *$p < 0.05$, ***$p < 0.001$ *versus* the control group. (C) Confocal laser scanning microscopy images of HepG2 cells incubated with *FITC-FYGL* for 4 h in the absence or presence of inhibitor, chlorpromazine, nystatin, amiloride, LY294002, and genistein. The scale bar represents 50 μm.

Open Access Article. Published on 29 August 2017. Downloaded on 2/15/2026 8:58:24 PM.
This article is licensed under a Creative Commons Attribution-NonCommercial 3.0 Unported Licence.

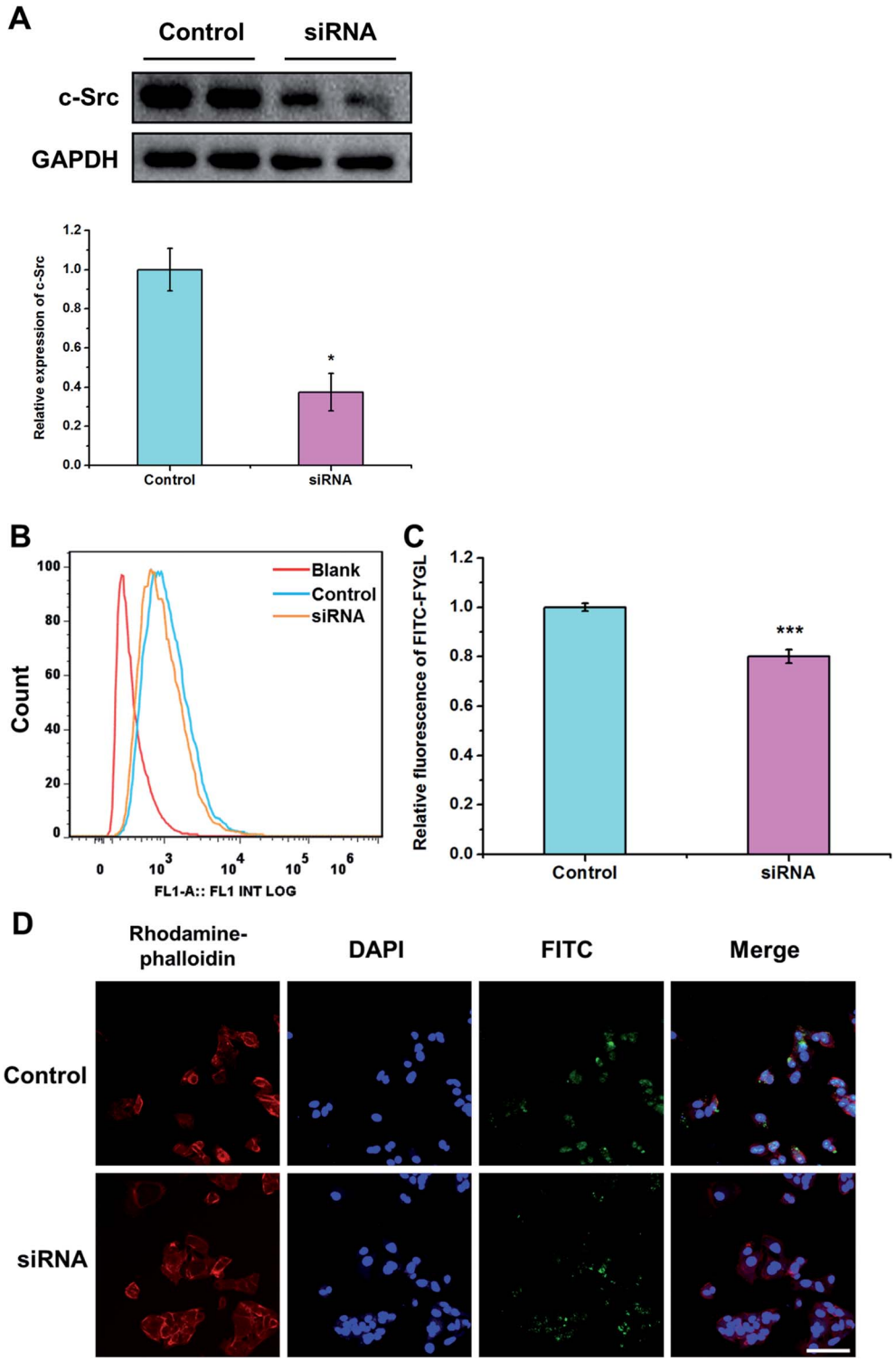

Fig. 6 (A) Western blot of c-Src protein in the control group and in siRNA transfected group. Data are presented as mean ± SD ($n = 3$). *$p < 0.05$ *versus* the control group. (B) FCM shows the peak position of 100 μg mL^{-1} *FITC-FYGL* in siRNA transfected HepG2 cells in channel FL1. (C) The relative fluorescent intensity of *FITC-FYGL* in siRNA transfected HepG2 cells. (D) Confocal laser scanning microscopy images of siRNA transfected HepG2 cells incubated with *FITC-FYGL* for 4 h. The scale bar represents 50 μm. Data are presented as mean ± SD ($n = 3$). ***$p < 0.001$ *versus* the control group.

This journal is © The Royal Society of Chemistry 2017

Open Access Article. Published on 29 August 2017. Downloaded on 2/15/2026 8:58:24 PM.
This article is licensed under a Creative Commons Attribution-NonCommercial 3.0 Unported Licence.

3.3 Intracellular uptake of *FYGL*

Fig. 3 shows the relative fluorescent intensity of green FITC-labeled *FYGL*, *FITC-FYGL*, at different concentrations by FCM analysis. The peak position in the *x*-axis moved towards right as the *FITC-FYGL* concentration increased from 25 to 200 μg mL^{-1} (Fig. 3A); the fluorescent intensity significantly increased in a dose-dependent manner (Fig. 3B). The confocal laser scanning microscopy images in Fig. 3C depict the intracellular uptake of *FITC-FYGL* in HepG2 cells.

3.4 The safe concentrations of *FITC-FYGL* and endocytic selective inhibitors in HepG2 cells

In order to investigate the endocytic mechanism, the safety of *FITC-FYGL* and the applied endocytic selective inhibitors for cells is necessary. The safety of *FITC-FYGL* and the selective inhibitors, genistein, amiloride, chlorpromazine, nystatin and LY294002, for HepG2 cells was tested using CCK-8. From Fig. 4, it is found that *FITC-FYGL* is safe for HepG2 cells in a wide concentration range; even at concentrations higher than 300 μg mL^{-1}, the cell is still viable up to 85%. The safety of the applied endocytic inhibitors was also tested (data not shown). Table 2 lists the safe concentrations of *FITC-FYGL* and the applied endocytic selective inhibitors in HepG2 cells, which will be used in the subsequent experiments.

3.5 Influence of endocytic selective inhibitors on *FYGL* uptake in HepG2 cells

Fig. 5A shows the FCM data of HepG2 cells (blank), the cells incubated with 100 μg mL^{-1} *FITC-FYGL* (control), and 100 μg mL^{-1} *FITC-FYGL* addition to preincubated 50 μg mL^{-1} chlorpromazine, 50 μg mL^{-1} nystatin, 100 μg mL^{-1} amiloride, 10 μg mL^{-1} LY294002, and 500 μg mL^{-1} genistein. From Fig. 5B, the fluorescence at $\lambda = 488$ nm was referred to that of blank group, and the *FITC-FYGL* fluorescence at $\lambda = 488$ nm in control group was normalized to 100. It was found that neither chlorpromazine nor nystatin had a significant inhibitory effect on endocytosis of *FYGL*, so the possibilities of clathrin-mediated endocytosis and caveolae/lipid-mediated endocytosis are excluded. However, the *FITC-FYGL* fluorescence in the groups with selective inhibitors of amiloride, LY294002 and genistein were all remarkably attenuated to different extents, compared with that in the control group, indicating that the uptake of *FITC-FYGL* in the cells was inhibited by amiloride, LY294002 and genistein. The results were also demonstrated by confocal laser scanning microscopy (Fig. 5C), which revealed that almost no green *FITC-FYGL* was observed in the cells with those inhibitors. Amiloride was reported to specifically inhibit macropinocytosis by lowering the submembraneous pH;[27] herein, the significant inhibition of the endocytic process of *FYGL* by amiloride indicated that the cellular uptake of *FYGL* was regulated by macropinocytosis. Macropinocytosis requires several kinases to activate numerous signaling pathways, which coordinate the formation of a macropinosome.[28] Genistein can inhibit either tyrosine kinases or caveolae pinching to regulate endocytosis.[22] In this study, the caveolae/lipid-mediated endocytosis of *FYGL* was excluded because nystatin did not inhibit *FYGL* entering the cells (Fig. 5); thus genistein may work on the inhibition of tyrosine kinase activity to block the uptake of *FYGL*.

As a quercetin analogue, LY294002 is widely used to specifically inhibit PI3K activity and macropinosome formation.[29,30] PI3K activity in the process of membrane ruffling affects the formation of macropinosomes and phagosomes, especially the closure of ruffles and pseudopodia, in addition to the influence on the roles of insulin and insulin growth factor-1 in signal transduction.[31–33] Herein, LY294002 down-regulated the uptake of *FYGL* in HepG2 cells, indicating that the uptake process might involve the PI3K cascade.

3.6 Endocytosis of *FYGL* mediated by c-Src protein

c-Src is a non-receptor tyrosine kinase and the upstream protein of PI3K, modulating ruffling in the early stages of phagocytosis.[18,34,35] Thus, inhibition of c-Src activity blocks the macropinocytosis process.[33] From Fig. 6A, HepG2 cells transfected with siRNA inhibited the expression of c-Src to a remarkable extent, compared with control group. The uptake of *FYGL* in HepG2 cells was also attenuated, which was demonstrated by FCM and the confocal laser scanning microscopy images in Fig. 6B–D. The results indicate that the endocytosis of *FYGL* in HepG2 cells is possibly on the c-Src/PI3K cascade involved in the macropinocytosis process.

3.7 Intracellular co-localization of *FYGL* and dextran

Dextran is used as a macropinocytosis tracer in endocytosis mechanism research.[15] The method of co-localization was used to prove that *FYGL* and dextran enter the cell *via* the same endocytosis pathway, if both compounds are overlaid in the cell. From the images in Fig. 7, we can observe that when *FYGL* and dextran were cultured in HepG2 cells, they were co-localized in the cells, and the merged image of *FYGL* (green, FITC labelled) and dextran (red, TRITC labelled) showed orange cells. The results demonstrated again that the uptake of *FYGL* in HepG2 cells was mainly through macropinocytosis and also identified the result of Fig. 3C.

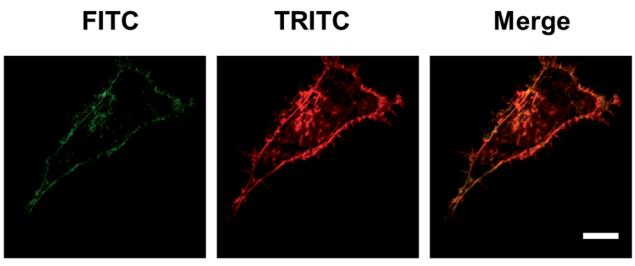

Fig. 7 Confocal laser scanning microscopy images of HepG2 cells incubated with *FITC-FYGL* for 4 h and TRITC-dextran for 10 min. The scale bar represents 10 μm.

Open Access Article. Published on 29 August 2017. Downloaded on 2/15/2026 8:58:24 PM.
This article is licensed under a Creative Commons Attribution-NonCommercial 3.0 Unported Licence.

4. Conclusions

In conclusion, we demonstrated that *FYGL* in aqueous solutions existed as aggregates with particle sizes in the range 400–1000 nm, and could be absorbed by HepG2 cells *via* the macropinocytosis mechanism. Moreover, we excluded clathrin-mediated endocytosis and caveolae/lipid-mediated endocytosis of *FYGL* by the pharmacologically selective inhibitor approach and proved that macropinocytosis mediated by c-Src/PI3K cascades was the preferred endocytic route. *FYGL* is a multidomain peptide that contains a polysaccharide and peptide domain and can potentially play multiple roles in the treatment of diseases. The specific structure of *FYGL* is an ideal case of bottom-up design where the modulation of chemical structure leads to controlled self-assembly and nanostructure, and eventually control of biological functions.[36] Our study provided the uptake basis of *FYGL* for efficient hypoglycemic action. The functional mechanism of the signaling pathway *in vivo* will be reported in the future.

Authors' contribution

ZY and FW performed the experiments and statistical analysis, ZY and PZ designed the experiments and wrote the manuscript, and HJY and PZ provided the funds.

Conflicts of interest

The authors declare the researchers in this study have no conflict of interest.

Acknowledgements

This study was supported by the Natural Science Foundation of China (No. 21374022 and 81374032).

References

1 C. Taghibiglou, F. Rashid-Kolvear, S. C. Van Iderstine, H. Le-Tien, I. G. Fantus, G. F. Lewis and K. Adeli, *J. Biol. Chem.*, 2002, **277**, 793–803.
2 M. Elchebly, P. Payette, E. Michaliszyn, W. Cromlish, S. Collins, A. L. Loy, D. Normandin, A. Cheng, J. Himms-Hagen, C. C. Chan, C. Ramachandran, M. J. Gresser, M. L. Tremblay and B. P. Kennedy, *Science*, 1999, **283**, 1544–1548.
3 T. O. Johnson, J. Ermolieff and M. R. Jirousek, *Nat. Rev. Drug Discovery*, 2002, **1**, 696–709.
4 M. Zaklos-Szyda, I. Majewska, M. Redzynia and M. Koziolkiewicz, *Curr. Top. Med. Chem.*, 2015, **15**, 2431–2444.
5 B. S. Teng, C. D. Wang, H. J. Yang, J. S. Wu, D. Zhang, M. Zheng, Z. H. Fan, D. Pan and P. Zhou, *J. Agric. Food Chem.*, 2011, **59**, 6492–6500.
6 H. T. Ma, J. F. Hsieh and S. T. Chen, *Phytochemistry*, 2015, **114**, 109–113.
7 D. Pan, L. Q. Wang, C. H. Chen, B. W. Hu and P. Zhou, *Carbohydr. Polym.*, 2015, **117**, 106–114.
8 C. Orellana-Tavra, S. A. Mercado and D. Fairen-Jimenez, *Adv. Healthcare Mater.*, 2016, **5**, 2261–2270.
9 T.-G. Iversen, T. Skotland and K. Sandvig, *Nano Today*, 2011, **6**, 176–185.
10 P. Zhao, M. Cao, L. N. Song, H. Wu, K. Hu, B. Chen, Q. W. Wang and N. Gu, *RSC Adv.*, 2016, **6**, 96635–96643.
11 W. H. Lewis, *Bull. Johns Hopkins Hosp.*, 1931, **49**, 17–27.
12 M. C. Kerr and R. D. Teasdale, *Traffic*, 2009, **10**, 364–371.
13 A. T. Jones, *J. Cell. Mol. Med.*, 2007, **11**, 670–684.
14 J. A. Swanson and C. Watts, *Trends Cell Biol.*, 1995, **5**, 424–428.
15 S. Elmquist, R. Libelius, G. Lawoko and S. Tagerud, *Muscle Nerve*, 1992, **15**, 876–884.
16 R. J. Jones, V. G. Brunton and M. C. Frame, *Eur. J. Cancer*, 2000, **36**, 1595–1606.
17 B. R. Wong, D. Besser, N. Kim, J. R. Arron, M. Vologodskaia, H. Hanafusa and Y. Choi, *Mol. Cell*, 1999, **4**, 1041–1049.
18 A. Aderem and D. M. Underhill, *Annu. Rev. Immunol.*, 1999, **17**, 593–623.
19 L. H. Wang, K. G. Rothberg and R. G. W. Anderson, *J. Cell Biol.*, 1993, **123**, 1107–1117.
20 C. K. Payne, S. A. Jones, C. Chen and X. Zhuang, *Traffic*, 2007, **8**, 389–401.
21 M. Koivusalo, C. Welch, H. Hayashi, C. C. Scott, M. Kim, T. Alexander, N. Touret, K. M. Hahn and S. Grinstein, *J. Cell Biol.*, 2010, **188**, 547–563.
22 L. Pelkmans, D. Puntener and A. Helenius, *Science*, 2002, **296**, 535–539.
23 P. Khandelwal, W. G. Ruiz and G. Apodaca, *EMBO J.*, 2010, **29**, 1961–1975.
24 Y. B. Tewari, M. M. Miller, S. P. Wasik and D. E. Martire, *J. Chem. Eng. Data*, 1982, **27**, 451–454.
25 L. Jiang, L. Wang, M. Guo, G. Yin and R.-Y. Wang, *Sens. Actuators, B*, 2011, **156**, 825–831.
26 Y. Katayama, *Bull. Chem. Soc. Jpn.*, 2017, **90**, 12–21.
27 M. A. West, M. S. Bretscher and C. Watts, *J. Cell Biol.*, 1989, **109**, 2731–2739.
28 Y. Egami, T. Taguchi, M. Maekawa, H. Arai and N. Araki, *Front. Physiol.*, 2014, **5**, 374.
29 C. J. Vlahos, W. F. Matter, K. Y. Hui and R. F. Brown, *J. Biol. Chem.*, 1994, **269**, 5241–5248.
30 N. Araki, M. Hamasaki, Y. Egami and T. Hatae, *Cell Struct. Funct.*, 2006, **31**, 145–157.
31 N. Araki, M. T. Johnson and J. A. Swanson, *J. Cell Biol.*, 1996, **135**, 1249–1260.
32 K. Kotani, K. Yonezawa, K. Hara, H. Ueda, Y. Kitamura, H. Sakaue, A. Ando, A. Chavanieu, B. Calas, F. Grigorescu, M. Nishiyama, M. D. Waterfield and M. Kasuga, *EMBO J.*, 1994, **13**, 2313–2321.
33 S. Wennstrom, P. Hawkins, F. Cooke, K. Hara, K. Yonezawa, M. Kasuga, T. Jackson, L. Claessonwelsh and L. Stephens, *Curr. Biol.*, 1994, **4**, 385–393.
34 M. Mettlen, A. Platek, P. Van Der Smissen, S. Carpentier, M. Amyere, L. Lanzetti, P. de Diesbach, D. Tyteca and P. J. Courtoy, *Traffic*, 2006, **7**, 589–603.
35 M. Okada and H. Nakagawa, *J. Biol. Chem.*, 1989, **264**, 20886–20893.
36 A. N. Moore and J. D. Hartgerink, *Acc. Chem. Res.*, 2017, **50**, 714–722.

 This journal is © The Royal Society of Chemistry 2017